

# Improved Irreversibility Behaviour and Critical Current Density in MgB<sub>2</sub>-Diamond Nanocomposites

**Author/Contributor:**

Zhao, Yong; Cheng, Cui; Rui, X; Zhang, H; Munroe, Paul; Zeng, H; Koshizuka, N; Murakami, M

**Publication details:**

Applied Physics Letters  
v. 83  
Chapter No. 14  
pp. 2916-2918  
0003-6951 (ISSN)

**Publication Date:**

2003

**Publisher DOI:**

<http://dx.doi.org/10.1063/1.1606884>

**License:**

<https://creativecommons.org/licenses/by-nc-nd/3.0/au/>

Link to license to see what you are allowed to do with this resource.

Downloaded from <http://hdl.handle.net/1959.4/39060> in <https://unsworks.unsw.edu.au> on 2024-03-03

## Improved irreversibility behavior and critical current density in MgB<sub>2</sub>-diamond nanocomposites

Y. Zhao<sup>a)</sup> and C. H. Cheng

*School of Materials Science and Engineering, University of New South Wales, Sydney 2052, NSW, Australia and State Key Lab for Mesophysics, Department of Physics, Peking University, Beijing 100871, China*

X. F. Rui and H. Zhang

*State Key Lab for Mesophysics, Department of Physics, Peking University, Beijing 100871, China*

P. Munroe

*School of Materials Science and Engineering, University of New South Wales, Sydney 2052, NSW, Australia*

H. M. Zeng

*Key Laboratory of Polymeric Composites and Functional Materials, The Ministry of Education, Zhongshan University, Guangzhou, 510275, People's Republic of China*

N. Koshizuka and M. Murakami

*Superconductivity Research Laboratory, ISTEK, 1-10 13 Shinonome, Koto-ku, Tokyo, 135-0062, Japan*

(Received 10 February 2003; accepted 8 July 2003)

MgB<sub>2</sub>-diamond nanocomposite superconductors have been synthesized by addition of nanodiamond powder. Microstructural analysis shows that the nanocomposite superconductor consists of tightly packed MgB<sub>2</sub> nanograins (~50–100 nm) with highly dispersed and uniformly distributed diamond nanoparticles (~10–20 nm) inside the grains. The  $J_c$ - $H$  and  $H_{irr}$ - $T$  characteristics have been significantly improved in this MgB<sub>2</sub>-diamond nanocomposite, compared to MgB<sub>2</sub> bulk materials prepared by other techniques. Also, the  $J_c$  value of  $1 \times 10^4$  A/cm<sup>2</sup> at 20 K and 4 T and the  $H_{irr}$  value of 6.4 T at 20 K have been achieved. © 2003 American Institute of Physics.

[DOI: 10.1063/1.1606884]

Since the discovery of superconductivity at 39 K in MgB<sub>2</sub>,<sup>1</sup> significant progress has been made in improving the performance of MgB<sub>2</sub> materials.<sup>2–4</sup> MgB<sub>2</sub> offers the possibility of wide engineering applications in the temperature range 20–30 K, where conventional superconductors, such as Nb<sub>3</sub>Sn and Nb–Ti alloy, cannot play any roles due to their low  $T_c$ . However, the realization of large-scale applications for MgB<sub>2</sub>-based superconductivity technology essentially relies on the improvement of the pinning behavior of MgB<sub>2</sub> in high fields. As it has poor grain connection and a lack of pinning centers, MgB<sub>2</sub> often exhibits a rapid decrease in critical current density,  $J_c$ , in high magnetic fields. Fortunately, through the formation of nanoparticle structures in bulk MgB<sub>2</sub><sup>2–4</sup> and thin films,<sup>5</sup> the problem of the poor grain connection can be solved, and the flux pinning force can also be significantly enhanced due to an increase of pinning centers served by grain boundaries. In order to improve further the performance of MgB<sub>2</sub>, it is necessary to introduce more pinning centers, especially those consisting of nanosized second-phase inclusions, which often provide strong pinning forces.

Nanodiamond, prepared by the detonation technique, has been widely used as an additive to improve the performance of various materials.<sup>6</sup> Yet, nanodiamond has never been used to increase the flux pinning force in MgB<sub>2</sub> superconductors until the present study. The high dispersibility of the nanodiamond powder makes it possible to form a high density of nanoinclusions in MgB<sub>2</sub> matrix. In this letter, we have prepared the MgB<sub>2</sub>-diamond nanocomposite, which consists of

tightly packed MgB<sub>2</sub> nanograins (~50–100 nm) with diamond nanoparticles (~10–20 nm) wrapped within the grains. This unique microstructure provides the composite with a good grain connection for the MgB<sub>2</sub> phase and a high density of flux-pinning centers served by the diamond nanoparticles. Compared to the MgB<sub>2</sub> bulk materials prepared with other techniques, the irreversibility line has been significantly improved and the  $J_c$  in high magnetic fields has been largely increased in the MgB<sub>2</sub>-diamond nanocomposite.

The MgB<sub>2</sub>-diamond nanocomposites with compositions of MgB<sub>2-x</sub>C<sub>x</sub> ( $x=0\%$ , 5%, 8%, and 10%) were prepared by solid-state reaction at ambient pressure. Mg powder (99% purity, 325 meshes), amorphous B powder (99% purity, submicron-size), and nanodiamond powder (10–20 nm) were mixed and ground in air for 1 h. An extra 2% of Mg powder was added in the starting materials to compensate the loss of Mg caused by high temperature evaporation. The mixed powders were pressed into pellets with dimensions of  $20 \times 10 \times 3$  mm<sup>3</sup> under a pressure of 800 kg/cm<sup>2</sup>, sandwiched into two MgO plates, sintered in flowing Ar at 800 °C for 2 h, and then quenched to room temperature in air. In order to compare the substitution effect of carbon in boron in MgB<sub>2</sub> with the additional effect of the nanodiamond in MgB<sub>2</sub>, a sample with an added 1.5 wt % of nanodiamond in MgB<sub>2</sub> was prepared. The sintering temperature and the sintering time for this sample were reduced respectively to 730 °C and 30 min in order to reduce the chemical reaction between the MgB<sub>2</sub> and the diamond. This sample has been referred to as 1.5 wt % C.

The crystal structure was investigated by powder x-ray diffraction (XRD) using an X'pert MRD diffractometer with

<sup>a)</sup>Electronic mail: y.zhao@unsw.edu.au

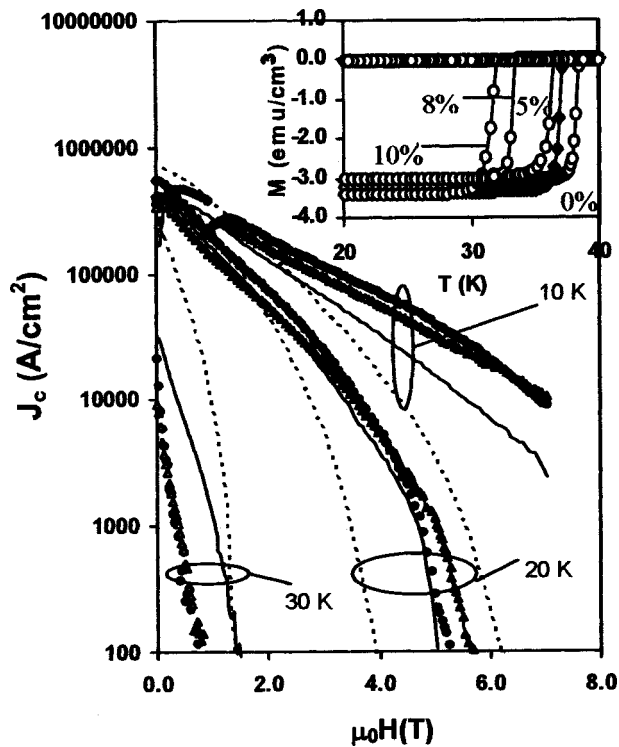


FIG. 1. Magnetic field dependence of  $J_c$  at 10, 20, and 30 K for  $\text{MgB}_{2-x}\text{C}_x$  with  $x=0\%$  (dashed lines), 5% (solid lines), 8% (solid circles), and 10% (open triangles). Inset: superconducting transition curves for the diamond-doped samples. The closed circles represent the results for the sample 1.5 wt % C.

$\text{Cu K}\alpha$  radiation. The microstructure was analyzed with a Philips CM200 field emission gun transmission electron microscope (FEGTEM). Dc magnetization measurements were performed in a superconducting quantum interference device (Quantum Design MPMS-7).  $J_c$  values were deduced from hysteresis loops using the Bean model. The sample's dimensions with typical values of  $0.7 \times 2.1 \times 2.7 \text{ mm}^3$  are used in the calculation of  $J_c$ . The values of the irreversibility field,  $H_{\text{irr}}$ , were determined from the closure of hysteresis loops with a criterion of  $10^2 \text{ A/cm}^2$ .

XRD results (not shown here) reveal a decrease of the lattice parameter along the  $a$ -axis due to a partial substitution of boron by carbon in  $\text{MgB}_2$ .<sup>7,8</sup> The substitution effect can also be reflected by the gradual decrease of  $T_c$  with increasing carbon content (see the inset of Fig. 1). The values of onset  $T_c$  for these carbon-substituted  $\text{MgB}_2$  samples are 38.6 K for  $x=0\%$ , 36.1 K for  $x=5\%$ , 33.0 K for  $x=8\%$ , and 31.3 K for  $x=10\%$ . The  $T_c$  for the sample 1.5 wt % C is 36.9 K, which is higher than that for the sample of  $x=5\%$  ( $T_c = 36.1 \text{ K}$ ), despite the former having a higher equivalent atomic percentage of carbon ( $x=5.4\%$ ).

Figure 1 shows the magnetic field dependence of  $J_c$  at 10, 20, and 30 K for the carbon-substituted  $\text{MgB}_2$  samples. At 30 K, the undoped  $\text{MgB}_2$  exhibits the highest  $J_c$  and the slowest decrease of  $J_c$  with  $H$ ; whereas the sample of  $x=10\%$  shows the lowest  $J_c$  and the quickest drop of  $J_c$  with  $H$ . It is evident that the  $J_c$ - $H$  behavior at 30 K for these samples is positively correlated to their  $T_c$  values. However, when the temperature decreases to the values far below  $T_c$ , a totally different situation appears. For example, at 10 and 20 K, the diamond-doped samples show a much better  $J_c$ - $H$  behavior. The  $J_c$  drops much more slowly in diamond-doped

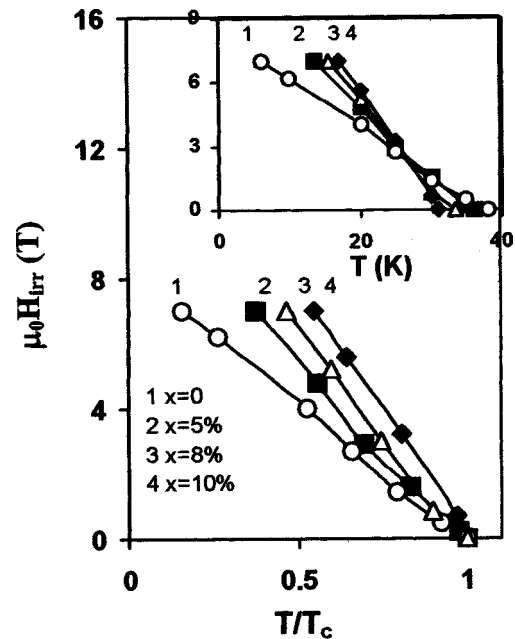


FIG. 2. Variation of  $H_{\text{irr}}$  with reduced temperature  $T/T_c$  for  $\text{MgB}_{2-x}\text{C}_x$  with  $x=0\%$ , 5%, 8%, and 10%. Inset:  $H_{\text{irr}}-T$  plot for the same data shown in the main figure.

samples than in pure  $\text{MgB}_2$ . The best  $J_c$  at 20 K is found in the sample of  $x=10\%$ , reaching a value of  $6 \times 10^3 \text{ A/cm}^2$  in a 4 T field, indicating that a strong flux pinning force exists in these diamond doped samples.

The  $H_{\text{irr}}-T$  relations for the diamond-substituted  $\text{MgB}_2$  are shown in the inset of Fig. 2. The  $H_{\text{irr}}(T)$  curves get steeper with increasing doping level. The best value of  $H_{\text{irr}}$  reaches 5.7 T at 20 K for the sample of  $x=10\%$ . As the  $T_c$  values vary with the diamond-doping level, only the  $H_{\text{irr}}-T$  relation cannot directly reflect the intrinsic irreversibility behavior for the samples of different doping levels. In the main panel of Fig. 2, the temperature dependence of  $H_{\text{irr}}$  is replotted using a reduced temperature,  $T/T_c$ . It is evident that the irreversibility field shifts towards higher temperatures with the increase of the diamond-doping level. The result clearly shows that the diamond doping does enhance the flux pinning in  $\text{MgB}_2$  significantly.

However, the effect of diamond doping on the enhancement of flux pinning in  $\text{MgB}_2$  may be counterbalanced by its suppression on superconductivity, as clearly shown in the situation of  $T=30 \text{ K}$  (see Fig. 1). This counterbalancing effect may also exist at other temperatures, even when the effect of the  $J_c$  enhancement is dominant. The further increase of  $J_c$  depends critically on reducing the  $T_c$ -suppression effect in the  $\text{MgB}_2$ -diamond composite. This idea is confirmed by the results obtained in the diamond-added sample, 1.5 wt % C, which has a higher  $T_c$  than other diamond-doped samples (see inset of Fig. 1) and contains more nanodiamond inclusions as suggested by the XRD analysis and confirmed by our transmission electron microscopy analysis shown later. As shown in Fig. 4, the diamond-added sample shows a much better  $J_c$ - $H$  behavior than the carbon-substituted sample. Its  $J_c$  reaches  $1 \times 10^4 \text{ A/cm}^2$  at 20 K and 4 T, and its  $H_{\text{irr}}$  reach 6.4 T at 20 K. In fact, at all temperatures below 35 K, the  $J_c$ - $H$  behavior (results at 20 K are shown here only) and the  $H_{\text{irr}}-T$  relation (see the inset of Fig. 3) of the diamond-added sample are much better than

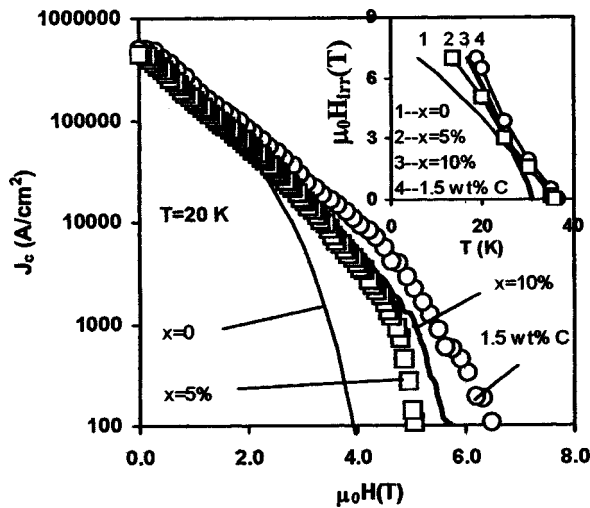


FIG. 3. Comparison of  $J_c$ - $H$  relations at 20 K for diamond-added  $\text{MgB}_2$  sample 1.5 wt % C with diamond-substituted  $\text{MgB}_2$ . The atomic percentages of carbon in the sample 1.5 wt % C and the sample of  $x=5\%$  are almost the same. Inset:  $H_{\text{irr}}-T$  relations for the same samples shown in the main figure.

those of other samples in this study.

Figure 4 shows the typical results from microstructural analysis for the diamond-substituted  $\text{MgB}_2$  and diamond-added  $\text{MgB}_2$  samples. The diamond-substitutional sample mainly consists of relatively large  $\text{MgB}_2$  grains ( $\sim 1 \mu\text{m}$  or so in size) with a high density of dislocations. In some areas, discrete nanosized particles can be seen [Figs. 4(a) and 4(b)]. The diamond-added sample mainly consists of two kinds of nanoparticles:  $\text{MgB}_2$  grains with a size of 50–100 nm and diamond particles with a size of 10–20 nm [see Fig. 4(c)]. In fact, this diamond-added  $\text{MgB}_2$  forms a typical nanocomposite material. The nanodiamond particles are inserted into the  $\text{MgB}_2$  grains. As the  $ab$  plane coherence length of  $\text{MgB}_2$  is about 6–7 nm,<sup>9</sup> these 10–20 nm-sized diamond inclusions, with a high density, are ideal flux pinning centres and are responsible for the high performance in our samples.

The significant improvement of  $J_c$  and  $H_{\text{irr}}$  in the nanodiamond-added samples (1.5 wt %) can be attributed to their nanocomposite structure which consists of two kinds of nanoparticles:  $\text{MgB}_2$  grains with a size of 50–100 nm and diamond particles with a size of 10–20 nm. The enhanced number of grain boundaries associated with the smaller grain size can enhance the flux pinning, as reported previously.<sup>2–5</sup>

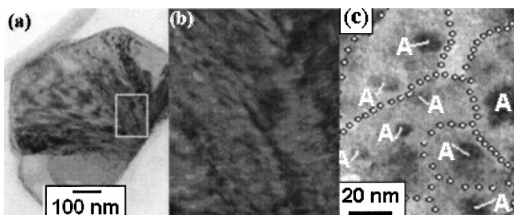


FIG. 4. FEGTEM micrographs for (a) a typical grain ( $\sim 1 \mu\text{m}$ ) of diamond substituted  $\text{MgB}_2$  with  $x=5\%$  which shows the high density of dislocations (dark stripes) in the sample; (b) an enlarged view of the dislocations in Fig. 4(a); (c) diamond added  $\text{MgB}_2$  with the carbon content of 1.5 wt %. The grain boundaries of  $\text{MgB}_2$  are indicated by the guidelines. The diamond nanoparticles are marked by letter A beside it (for small ones) or on the particles (for big ones). The atomic percentages of carbon in these two samples are almost the same.

However, only this factor cannot fully explain the experimental results because the enhancement of flux pinning in the nanodiamond-added samples (1.5 wt %) is even much better than that in the Ti-doped  $\text{MgB}_2$ <sup>2–4</sup> where the average grain size of  $\text{MgB}_2$  reaches 8–10 nm. This indicates that there may be other mechanisms of flux pinning enhancement in the present system. One of the most likely candidates is the diamond nanoparticles which may play a similar role as  $\text{Y}_2\text{O}_3$  nanoparticles did in  $\text{Y}_2\text{O}_3$ -doped  $\text{MgB}_2$ .<sup>10</sup> It is worth noting that, compared to the  $\text{Y}_2\text{O}_3$   $\text{Y}_2\text{O}_3$ -doped  $\text{MgB}_2$  the nanodiamond-added samples (1.5 wt %) has a higher  $J_c$  and  $H_{\text{irr}}$ . This may be due to the advantage of the nanodiamond whose lattice contact (for the cubic diamond  $a=0.356 \text{ nm}$ ) is very close to the  $c$  axis of  $\text{MgB}_2$  ( $c=0.352 \text{ nm}$ ). Therefore, these diamond nanoparticles may provide nucleation centres for  $\text{MgB}_2$  and are tightly bound to them. It has been reported that some undoped  $\text{MgB}_2$  samples with a slight grain texture also show a high  $J_c$  and  $H_{\text{irr}}$  (see, for example, Narozhnyi *et al.*),<sup>11</sup> suggesting that achieving a textured microstructure is another effective way to improve  $J_c$  of  $\text{MgB}_2$  because of a slight anisotropy existing in this system. Accordingly, it is expected that the performance of the  $\text{MgB}_2$ -diamond nanocomposite may be further improved by optimizing the microstructure and the doping levels.

In summary, we have synthesized a  $\text{MgB}_2$ -diamond nanocomposite superconductor by adding nanodiamond powder into  $\text{MgB}_2$ . The nanocomposite consists of tightly packed  $\text{MgB}_2$  nanograins ( $\sim 50$ – $100 \text{ nm}$ ) with diamond nanoparticles ( $\sim 10$ – $20 \text{ nm}$ ) inserted inside these grains. The  $J_c$ - $H$  and  $H_{\text{irr}}-T$  characteristics have been significantly improved in this  $\text{MgB}_2$ -diamond nanocomposite, in comparison with  $\text{MgB}_2$  bulk materials prepared with other techniques.

The authors are grateful to Sisi Zhao for her helpful discussion in preparing the manuscript. This work was supported in part by the University of New South Wales (Goldstar Award for C.H.C.). Financial support from the Ministry of Science and Technology of China (NKBRF-G19990646) is also acknowledged.

- <sup>1</sup>J. Nagamatsu, N. Nakagawa, T. Muranaka, Y. Zenitani, and J. Akimitsu, *Nature* (London) **410**, 63 (2001).
- <sup>2</sup>Y. Zhao, Y. Feng, C. H. Cheng, L. Zhou, Y. Wu, T. Machi, Y. Fudamoto, N. Koshizuka, and M. Murakami, *Appl. Phys. Lett.* **79**, 1154 (2001).
- <sup>3</sup>Y. Zhao, D. X. Huang, Y. Feng, C. H. Cheng, T. Machi, N. Koshizuka, and M. Murakami, *Appl. Phys. Lett.* **80**, 1640 (2002).
- <sup>4</sup>Y. Zhao, Y. Feng, T. Machi, C. H. Cheng, D. X. Huang, Y. Fudamoto, N. Koshizuka, and M. Murakami, *Europhys. Lett.* **57**, 437 (2002).
- <sup>5</sup>C. B. Eorn, M. K. Lee, J. H. Choi, L. J. Belenky, X. Song, L. D. Cooley, M. T. Maus, S. Patnaik, J. Jiang, M. Rikel, A. Polyanskii, A. Gurevich, X. Y. Cai, S. D. Bu, S. E. Babcock, E. E. Hellstrom, D. C. Larbalestier, N. Rogado, K. A. Regan, M. A. Hayward, T. He, J. S. Slusky, K. Inumaru, M. K. Haas, and R. J. Cava, *Nature* (London) **411**, 558 (2001).
- <sup>6</sup>Q. Chen and S. Yun, *Mater. Res. Bull.* **35**, 1915 (2000).
- <sup>7</sup>T. Takenobu, T. Ito, D. H. Chi, K. Prassides, and Y. Iwasa, *Phys. Rev. B* **64**, 134513 (2001).
- <sup>8</sup>W. Mickelson, J. Cumings, W. Q. Han, and A. Zettl, *Phys. Rev. B* **65**, 052505 (2002).
- <sup>9</sup>M. Xu, H. Kitazawa, Y. Takano, J. Ye, K. Nishida, H. Abe, A. Matsushita, N. Tsujii, and G. Kido, *Appl. Phys. Lett.* **79**, 2779 (2001).
- <sup>10</sup>J. Wang, Y. Bugoslavsky, A. Berenov, L. Cowey, A. D. Caplin, L. F. Cohen, J. L. MacManus Driscoll, L. D. Cooley, X. Song, and D. C. Larbalestier, *Appl. Phys. Lett.* **81**, 2026 (2002).
- <sup>11</sup>V. N. Narozhnyi, G. Fucks, A. Handstein, A. Gumbel, J. Eckert, K. Nenkov, D. Hinz, O. Gutfleisch, A. Walte, L. N. Bogacheva, I. E. Kostyleva, K.-H. Muller, and L. Schultz, *cond-mat/0206513*.